Nanocomposites

Original Research Paper

Nanocomposite toughness, strength and stiffness: role of filler geometry

Israel Greenfeld and H. Daniel Wagner*

Department of Materials and Interfaces, The Weizmann Institute of Science, Rehovot 76100, Israel

Abstract The toughness, strength and stiffness of nanocomposites are considered for the general case of hollow fillers with arbitrarily shaped cross-sections. The particular cases of nanotubes, thin wall general cylindrical fillers, and thin ribbons are examined. The toughness is expressed by the energy dissipated when the filler pulls out from the matrix during the composite fracture, taking into consideration the filler critical length. The study reveals how the properties of nanocomposites can be optimized by modulating the filler shape and dimensions, as well as the mechanical properties of the material and interface. The tradeoffs between toughness, strength and stiffness are analyzed in view of their different and sometimes opposite dependence on the material and geometric parameters. It is shown that when the filler is shorter than its critical length, typical of most current nanotubes, the toughness, strength and stiffness can be improved simultaneously by reducing the filler cross-sectional aspect ratio (wall thickness divided by diameter). The mechanical performance of composites reinforced by carbon nanotubes and microfibers is compared for several possible filler packing conformations, demonstrating the high potential of nanoreinforcement.

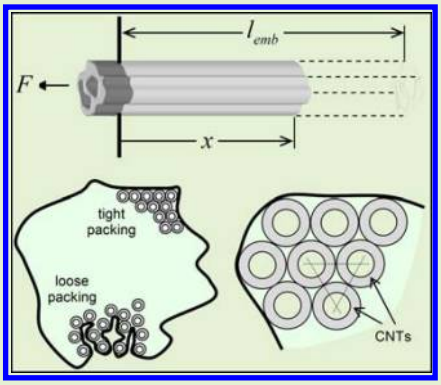

Keywords Nanocomposite, Toughness, Strength, Stiffness, Nanotube, CNT, CNTF, WSNT

Cite this article I. Greenfeld and H. D. Wagner: *Nanocomposites*, 2015, 1, 3-17

Introduction

Reinforcement at the nanoscale, using fillers like carbon nanotubes (CNTs), tungsten disulfide nanotubes (WSNTs) and molybdenum disulfide nanoplatelets (MSNPs), has the potential for improving the composite strength, stiffness and toughness compared to microscale reinforcement. Nanofillers could potentially be used in standard composite applications, as well as in confined spaces, thin polymer nanofilms[1,2] and electrospun polymer nanofibers.[3–5] Nanofillers such as carbon nanotubes possess strength and stiffness an order of magnitude higher than traditional microfillers like carbon microfibers.[6,7] Furthermore, the ratio of the filler's interfacial area to volume ($R/R^2 \sim R^{-1}$), which determines its load bearing capacity, becomes extremely large for nanofillers, 10^2–10^3 higher than microfillers. At the same time, nanofillers are often short and hollow, have arbitrarily shaped cross-sections, and form complex arrays and networks.[8]

It is the aim of the present study to generalize the modeling of the mechanical properties of hollow fillers, to those having an irregular cross-sectional shape, of which nanofillers are a typical example. Specifically, we demonstrate that the cross-sectional shape of a reinforcing filler has a significant influence on the overall mechanical performance of the composite, particularly so for nanocomposites in view of the effects of the filler's small size and diverse shapes and structures. For the purpose of this study, we assume uniform dispersion of the filler in the matrix and unidirectional alignment, both optimal conditions for enhanced performance.

We focus on the structural toughening properties of nanoreinforcement, for which there is growing evidence of improved mechanical performance.[3,9–11] The major mechanism contributing to toughening of reinforced composites is the energy dissipated when the filler is pulled out from the matrix through the fracture surface.[12] The pullout energy of nanotube reinforced composites was modeled by Wagner,[13,14] based on the classic models by Cottrell[15] and Kelly–Tyson[16] developed for solid fibers. We expand these models to encompass fillers with arbitrarily shaped cross-sections, including the distinct class of thin wall fillers. A starting point for the model is the filler critical length, the length above which the filler breaks rather than pulls out.

Also, the classic models by Piggott[17] and others for the strength and stiffness of composites are expanded for such

*Corresponding authors, email daniel.wagner@weizmann.ac.il and green_is@netvision.net.il

Received 28 August 2014; accepted 29 October 2014
DOI 10.1179/2055033214Y.0000000002

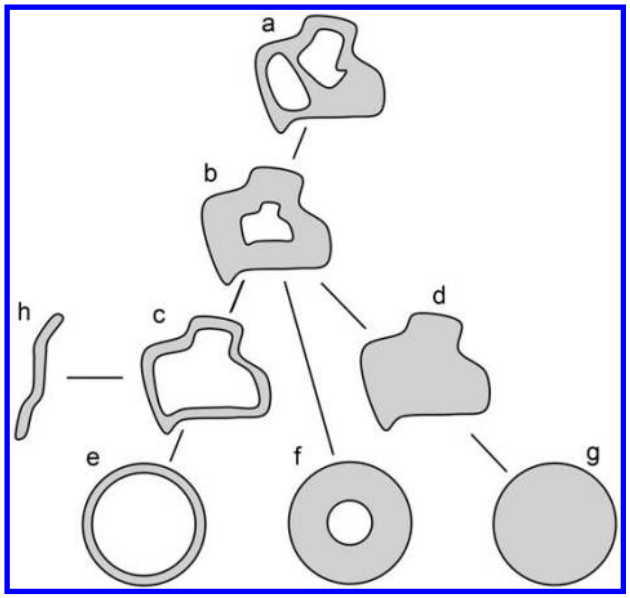

Figure 1 Categories of cross-sectional shapes of cylindrical fillers: *a* arbitrarily shaped outline and cavities (e.g. aligned NT bundle); *b* arbitrary shape, single cavity; *c* arbitrary shape, thin wall; *d* arbitrary shape, solid; *e* circular, thin wall (e.g. single wall nanotube); *f* circular, thick wall (e.g. multiwall nanotube); *g* circular, solid (e.g. fiber); *h* open shape, thin or thick wall (e.g. flat ribbon, graphene)

arbitrarily shaped fillers. The overall mechanical performance of the composite structure is presented as a tradeoff between the toughness, strength and stiffness, since these properties depend differently (and sometimes oppositely) on parameters such as the filler's length, cross-sectional shape, strength, stiffness and volume fraction, as well as the matrix and interface strength and stiffness. Finally, the performance of nano- and microreinforcements is compared for several composite structures with different filler packing schemes.

Effect of filler shape on critical length

The cross-section of an elongated reinforcing nanofiller may have diverse shapes, as illustrated in Fig. 1. In the most general case, a single filler has the form of a hollow *general cylinder* (a solid bounded by a right ruled closed surface),[18] whose cross-section has arbitrarily shaped outline and multiple cavities (Fig. 1*a*); a spun bundle of aligned hollow nanotubes is an example of such a filler (Appendix). An arbitrarily shaped filler may be solid (Fig. 1*d*), or have a thick wall (Fig. 1*b*) or a thin wall (Fig. 1*c*). A filler may have a circular cross-section, and its core may be solid as in a fiber (Fig. 1*g*), or hollow with a thin or thick wall, as in a single wall (Fig. 1*e*) or multiwall (Fig. 1*f*) nanotube. Finally, a thin or thick ribbon (Fig. 1*h*) is another category of a cylindrical filler.

We therefore seek to generalize our recently proposed toughness model[13,14] of a unidirectional filler, based on the pullout mechanism, to a wider class of cross-sectional shapes. We first focus on the critical length of a filler having an arbitrarily shaped cross-section.

Consider a hollow filler of the form of a general cylinder embedded in a matrix, with a material cross-sectional area a and an outer perimeter p. The longitudinal tensile stress in the filler $\sigma(x)$, and the interfacial stress between the filler and the matrix $\tau(x)$, acting on a differential element of the filler (Fig. 2), are expressed by

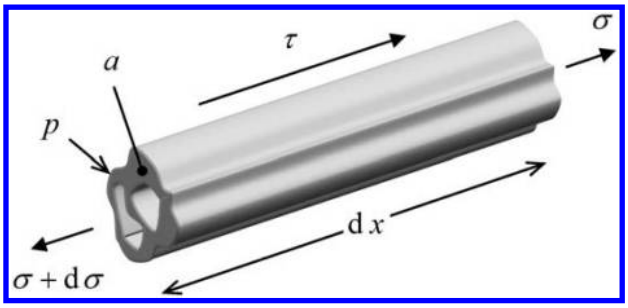

Figure 2 Tensile stress σ and interfacial stress τ acting on differential element d*x* of hollow filler with arbitrarily shaped cross-section, having perimeter *p* and material area *a*

$$p\tau(x)\,\mathrm{d}x = a[\sigma(x)+\mathrm{d}\sigma] - a\sigma(x) = a\,\mathrm{d}\sigma \tag{1}$$

where x is the distance from the filler edge. When the filler is long and its cavities are narrow, the matrix column embedded internally inside the filler is constrained by the relatively small displacement of the stiff filler, resulting in high matrix stresses close to the filler ends, leading to local breaking of the matrix. Therefore, the contribution of the internal matrix column to the stress in the filler is negligible. Furthermore, for nanofillers, the matrix material (e.g. polymer) is not likely to penetrate the cavities at all.

The CKT model[15,16] assumes that when the tensile load is applied, the interfacial stress reaches a constant value $\tau(x)=\tau_i$, corresponding to the yield strength of the matrix or the bonding strength between the filler and the matrix, whichever is lower. More specifically, according to Mallick,[19] this assumption is valid for a ductile matrix, which yields under a high interfacial stress and flows plastically with little or no strain hardening. Such an elastic perfectly plastic matrix maintains a constant yield strength, equal to the interfacial shear stress τ_i. By comparison, shear lag based models predict that in the filler central length the stress transfer is elastic rather than plastic, whereas in regions close to the filler edges the matrix may yield or debond.[17,20] For a ductile matrix, with a yield strength lower than the filler–matrix bonding strength, when the external stress is gradually increased, the matrix yielded regions expand from the filler edges toward the center, and the resulting shear lag stress profile approaches that of CKT. In case it is the filler–matrix bonding strength which is lower than the matrix yield strength, the interfacial shear stress τ_i is the friction stress caused by the compression applied by the matrix on the filler.

Integrating equation (1) with a constant interfacial stress, we obtain

$$\sigma(x) = \tau_i x\frac{p}{a},\quad \sigma(x) \le \sigma_f \tag{2}$$

where σ_f is the filler ultimate strength. Thus, the tensile stress in the filler $\sigma(x)$ grows linearly with the distance from its edges, until σ_f is reached and the filler breaks. This occurs when the filler is longer than a critical length l_c, obtained by substituting $x=l_c/2$ into equation (2)

$$l_c = \frac{2\sigma_f}{\tau_i}\frac{a}{p} \tag{3}$$

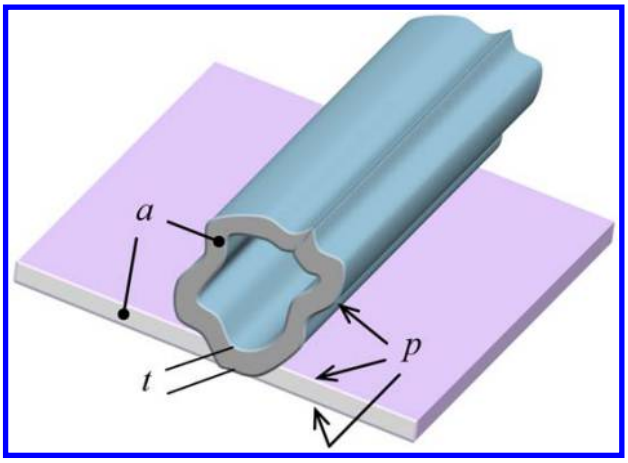

Figure 3 Analogy between thin wall arbitrarily shaped cylinder and thin ribbon: cylinder is spread out flat and forms ribbon with thickness *t*, width *p*, total perimeter 2*p* (both sides) and cross-sectional area *a*; ribbon has half critical length of cylinder, assuming double sided bonding to matrix, and its critical length is independent of its width

In the case of a thin wall hollow filler having a wall thickness t (Figs. 1*c* and 3), the ratio $a/p \cong t$, and therefore

$$l_c^{thin} \cong \frac{2\sigma_f t}{\tau_i} \tag{4}$$

regardless of the cross-section shape, whether circular, elliptic or warped.

Note that the thin wall critical length does not depend on the filler lateral size (i.e. width) but only on its thickness. This outcome is clarified when spreading out the general cylinder into an equivalent flat ribbon (Fig. 3), for which $a/p \cong t/2$ and the critical length is $l_c = \sigma_f t/\tau_i$, independent of the ribbon width p. The critical length of the equivalent ribbon is half that of the closed shape because its bonding to the matrix is double-sided. Hence, possibly, the use of ribbons (e.g. graphene) may be beneficial when a shorter critical length is desired.

For a circular hollow tube (e.g. a nanotube), with an outer diameter D, inner diameter d and wall thickness $t = (D-d)/2$, we define the following function of the cross-sectional aspect ratio t/D

$$A_{tD} \equiv \frac{a}{a_{tot}} = \frac{(D^2-d^2)}{D^2} = 4\frac{t}{D}\left(1-\frac{t}{D}\right) \tag{5}$$

This function, which represents the ratio between the filler's material area a and its total area a_{tot} (the area bounded by the filler perimeter p), ranges from $4t/D \cong 0$ for a thin wall tube ($t \ll D$) to 1 for a solid fiber ($t = D/2$). The ratio a/p for circular cylinders is therefore

$$\frac{a}{p} = \frac{\pi(D^2-d^2)}{4\pi D} = t\left(1-\frac{t}{D}\right) = \frac{D}{4}A_{tD} \tag{6}$$

The corresponding critical length from equation (3) is

$$l_c = \frac{2\sigma_f t}{\tau_i}\left(1-\frac{t}{D}\right) = \frac{\sigma_f D}{2\tau_i}A_{tD} = l_c^{solid}A_{tD} \tag{7}$$

which reduces to the known expression $l_c^{solid} = \sigma_f D/(2\tau_i)$ for a solid fiber, and to $2\sigma_f t/\tau_i$ of equation (4) for a thin wall tube.

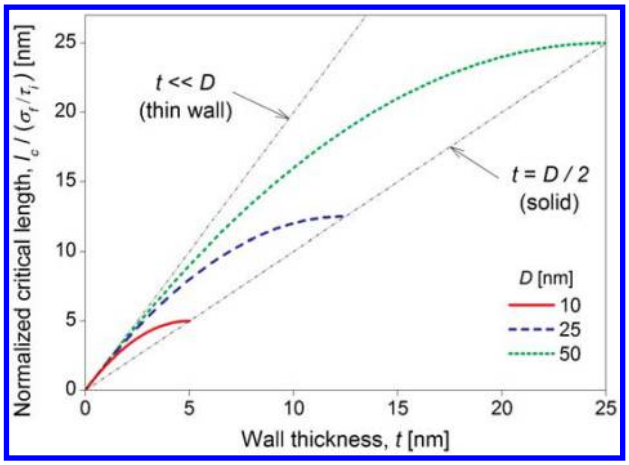

Figure 4 Normalized critical length $l_c/(\sigma_f/\tau_i)$ vs. wall thickness *t* and outer diameter *D* of circular hollow tube (equation (7)): multiply by $\sim 10^3$ to obtain the order of l_c for a CNT; bounds for thin wall and solid cylinders are marked; lowest possible wall thickness of CNT is that of single wall that is 0.34 nm

A tube with thicker wall, larger diameter and higher tensile strength has a longer critical length, and *vice versa* (Fig. 4). For example, the scale of the critical length of a carbon nanotube is two to three orders of magnitude lower than that of a carbon fiber (using equation (7) with 10^1 higher σ_f, 10^{-3} smaller D and $A_{tD} < 1$). When the filler length is longer than its critical length (a typical case in microscale reinforcement), it is desirable to increase the critical length in order to optimize toughness. On the other hand, as will be shown later (see also Ref. 13), when the filler length is shorter than its critical length (a typical case in nanoscale reinforcement), it is desirable to reduce the critical length, in other words to decrease the wall thickness, diameter and tensile strength and increase the interfacial strength.

The aspect function A_{tD}, depicted in Fig. 5, is useful for comparing the critical length (and as will be seen, the pullout energy) of a hollow tube to a solid fiber having the same external diameter. The higher the aspect ratio (thicker tube wall and/or smaller diameter), the longer the critical length of the tube with respect to a solid fiber, and *vice versa*. Note that $l_c \leq l_c^{solid}$ in all cases.

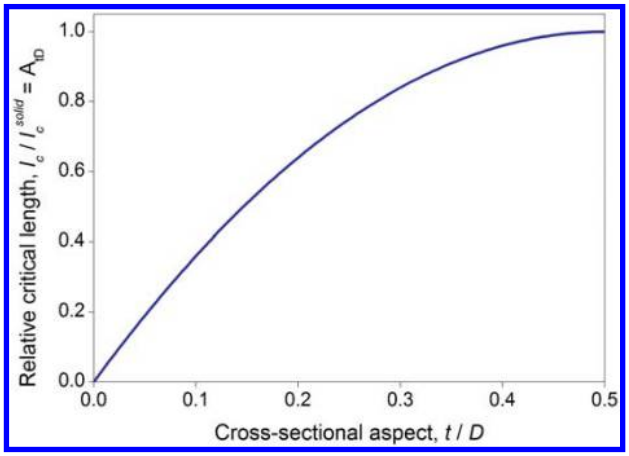

Figure 5 Relative critical length l_c/l_c^{solid} (or aspect ratio function A_{tD}) versus cross-sectional aspect ratio *t*/*D* of circular hollow tube (equations (7) and (5))

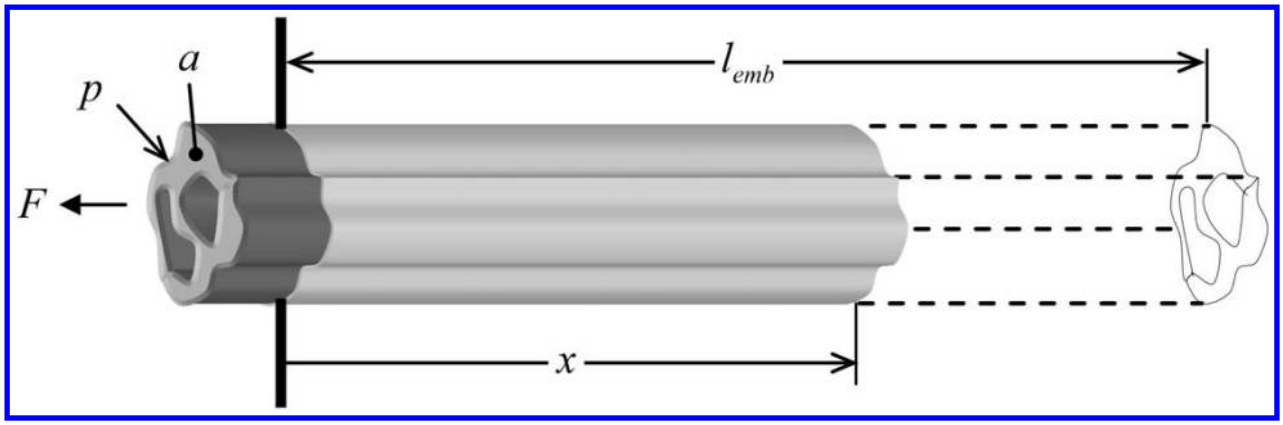

Figure 6 Force *F* pulling out hollow filler that has initial embedded length l_{emb} in matrix: filler has arbitrarily shaped cross-section with perimeter *p* and material area *a*

Effect of filler shape on pullout energy

The energy absorbed during pulling out of a unidirectional elongated filler from an embedding soft matrix is generally the major contributor to toughening of a composite structure. The following analysis generalizes the toughness model[13] to an arbitrarily shaped hollow filler, representative of a wide class of cross-sectional shapes (Fig. 1), and expands on thin wall hollow filler (Fig. 1*c*) and open filler (Fig. 1*h*), as well as circular hollow filler (Fig. 1*e* and *f*), with a solid fiber (Fig. 1*g*) as a particular case.

The force needed to pull out a hollow filler embedded length x in a soft matrix, when the filler has the form of a general cylinder with perimeter p, is $F(x)=px\tau_i$ (Fig. 6). The interfacial stress τ_i is the yield strength of the matrix or the interfacial bonding, and is assumed constant as previously described. Thus, the work for a complete pullout of a filler that is initially embedded l_{emb} in the matrix is

$$W(l_{emb})=\int_0^{l_{emb}} F(x)\,dx=\frac{p\tau_i l_{emb}^2}{2} \tag{8}$$

As discussed in the previous section, when the filler is long and its cavities are narrow, the matrix column embedded internally (if any) in the filler's cavities does not pull out and does not transfer any load from the applied force, since it breaks at the filler ends during the onset of pullout (this break dissipates significantly less energy compared to the pullout energy).

The pullout work for N unidirectional such fillers, whose embedded length is evenly distributed from 0 to l_{emb}, is

$$\langle W\rangle=N\frac{\int_0^{l_{emb}} W(l_{emb})\,dl_{emb}}{\int_0^{l_{emb}} dl_{emb}}=N\frac{p\tau_i l_{emb}^2}{6} \tag{9}$$

Consider a composite's representative volume element (RVE), whose total cross-sectional area is A, encompassing the matrix area, the filler cumulative material area Na, and any cavities inside or outside the filler. Since the volume fraction of the filler in that RVE is $V_f=Na/A$, the number of fillers intersecting the fracture surface is on average

$$N=\frac{V_f A}{a} \tag{10}$$

independent of the filler length.

Using equations (9) and (10), the pullout energy area density (in short, pullout energy) is given by

$$G=\frac{\langle W\rangle}{A}=\frac{V_f\tau_i l_{emb}^2}{6}\frac{p}{a} \tag{11}$$

which can be rewritten in terms of the critical length by substituting the ratio p/a from equation (3)

$$G=\frac{V_f\sigma_f l_{emb}^2}{3l_c} \tag{12}$$

independent of the cross-section shape and whether it is hollow or not.

In the case of a filler whose length l is shorter than its critical length, for example as typical of most current nanotubes, the maximum embedded length is $l_{emb}=l/2$, and therefore

$$G=\frac{V_f\sigma_f l^2}{12l_c},\quad l<l_c \tag{13}$$

Note that this expression is universal for any cross-sectional shape. For a thin wall filler with a wall thickness t, we substitute l_c from equation (4)

$$G_{thin}\cong\frac{V_f\tau_i l^2}{24t},\quad l<l_c \tag{14}$$

independent of the cross-section shape and lateral size. In the case of a thin wall ribbon-shaped filler (e.g. graphene), assuming the same interfacial strength (which may not necessarily be the case), the pullout energy will increase by a factor of 2. Substituting l_c for a circular cross-section from equation (7) into equation (13)

$$G=\frac{V_f\tau_i l^2}{24t(1-t/D)}=\frac{V_f\tau_i l^2}{6D}A_{tD}^{-1},\quad l<l_c \tag{15}$$

which reduces to $G_{solid}=V_f\tau_i l^2/(6D)$ for a solid fiber (using equation (5) with $t=D/2$, leading to $A_{tD}=1$).

The pullout energy in this filler length domain is invariant with respect to the filler ultimate strength σ_f. However, when σ_f is very high, the pullout energy will not grow indefinitely with the filler length l because of fracture mechanics considerations arising from inherent flaws in the filler. Consequently, the filler will tend to break at the flaw nearest to the matrix fracture plane, where the filler stress is highest, and, according to Piggott,[17] the pullout energy will

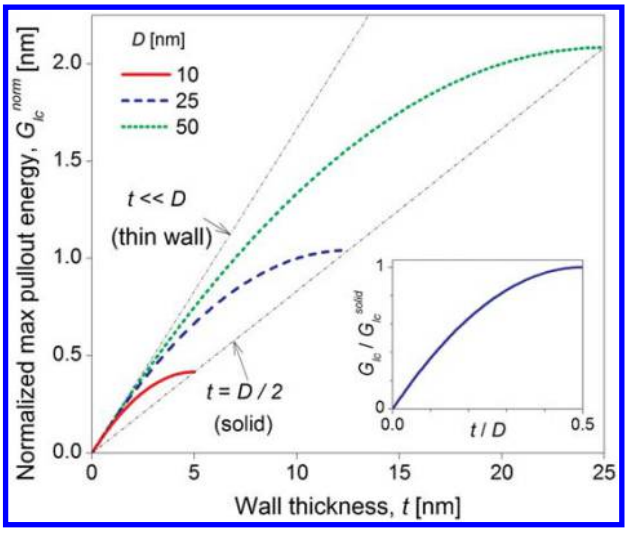

Figure 7 Maximum pullout energy G_{lc} versus wall thickness t and outer diameter D of circular hollow tube (equation (21)): normalized energy $G_{lc}^{norm} = G_{lc}/(V_f\sigma_f^2/\tau_i)$, and relative energy G_{lc}/G_{lc}^{solid} (inset)

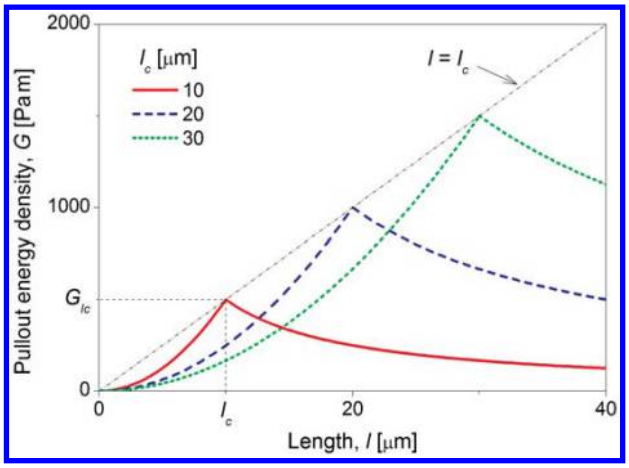

Figure 8 Pullout energy G as function of filler length l, for three values of critical length l_c (equations (13), (16) and (19)): $V_f\sigma_f/12 = 50$ MPa; holds for any cross-sectional shape

saturate at $G_{sat} = 2V_f\tau_i L^2/D$, where L is the filler fragment pullout length. The length L is inversely proportional to the density of flaws along the filler, derived from the flaw statistical distribution. Note the similarity between the expressions of G_{sat} and G_{solid}, obtained by substituting $l = 2\times 3^{1/2} L$.

In the case of a filler that is longer than its critical length, we observe two possible types of events: if the filler is embedded more than $l_c/2$ beyond the fracture surface in both directions, its stress exceeds the ultimate strength and it will break at the fracture surface,[15] dissipating a relatively low energy compared to pullout; if the filler is embedded less than $l_c/2$ in one of the two directions, it will pull out without breaking. Thus, only the latter event contributes to the pullout energy, and its probability of occurrence is l_c/l. Since the embedded length in that type of event ranges from 0 to $l_c/2$, we substitute $l_{emb} = l_c/2$ into equation (12), and adjust by the probability of occurrence

$$G = \frac{V_f\sigma_f(l_c/2)^2}{3l_c}\frac{l_c}{l} = \frac{V_f\sigma_f l_c^2}{12l},\quad l > l_c \tag{16}$$

Note that this expression is universal for any cross-sectional shape. For a thin wall filler having a wall thickness t, we substitute l_c from equation (4)

$$G_{thin} \cong \frac{V_f\sigma_f^3 t^2}{3\tau_i^2 l},\quad l > l_c \tag{17}$$

independent of the cross-section shape and lateral size. In the case of a thin wall ribbon shaped filler (e.g. graphene), the pullout energy will degrade by a factor of 4 (because of the term l_c^2 in equation (16)). Substituting l_c for a circular cross-section (equation (7))

$$G = \frac{V_f\sigma_f^3 t^2}{3\tau_i^2 l}\left(1-\frac{t}{D}\right)^2 = \frac{V_f\sigma_f^3 D^2}{48\tau_i^2 l}A_{tD}^2,\quad l > l_c \tag{18}$$

which reduces to $G_{solid} = V_f\sigma_f^3 D^2/(48\tau_i^2 l)$ for a solid fiber.

The maximum achievable pullout energy G_{lc} is obtained when the filler's length is equal to its critical length, or $l = l_c$ (in fact, l should be slightly shorter than l_c in order to ensure no filler breaking). Substituting $l_{emb} = l_c/2$ into equation (12)

$$G_{lc} = \frac{V_f\sigma_f l_c}{12} \tag{19}$$

which is universal for any cross-sectional shape. For a thin wall hollow filler with arbitrarily shaped cross-section, this expression reduces to (using equation (4))

$$G_{lc}^{thin} \cong \frac{V_f\sigma_f^2 t}{6\tau_i} \tag{20}$$

For a circular hollow tube (e.g. a nanotube), the maximum pullout energy is (using equation (7))

$$G_{lc} = \frac{V_f\sigma_f^2 D}{24\tau_i}A_{tD} = G_{lc}^{solid}A_{tD} \tag{21}$$

which reduces to $G_{lc}^{solid} = V_f\sigma_f^2 D/(24\tau_i)$ for a solid fiber. The dependence of G_{lc} on the cross-sectional geometry is depicted in Fig. 7. The maximum pullout energy cannot grow indefinitely with σ_f, and, as previously described, is bounded by the saturation energy G_{sat}, which depends on the density of filler flaws.

The pullout energies for the two filler length domains are depicted in Fig. 8. Similar plots are known in the literature for solid fibers, for example see Ref. 21; however, the current analysis demonstrates the universality of such plots with respect to any arbitrarily shaped hollow cross-sections.

Figure 8 demonstrates how the pullout energy can be increased when $l < l_c$: the preferred method, which yields the highest possible pullout energy for a given l_c, would be to increase l until it approaches l_c and the energy reaches its peak. If that is not possible, l_c can be reduced until it approaches l, achievable by (equation (7) and Fig. 4) using a filler with smaller wall thickness and/or lateral width, and/or by increasing the interfacial strength (e.g. by chemical functionalization of the filler). In the latter method, the energy will also reach a peak, but a lower peak than in the first method. For example (Fig. 8), suppose we have $l = 10$ μm and $l_c = 20$ μm: in the first method the energy will rise from 250 Pa m to 1000 Pa m by increasing l to 20 μm, while in the second method it will rise only to 500 Pa m by decreasing l_c to 10 μm.

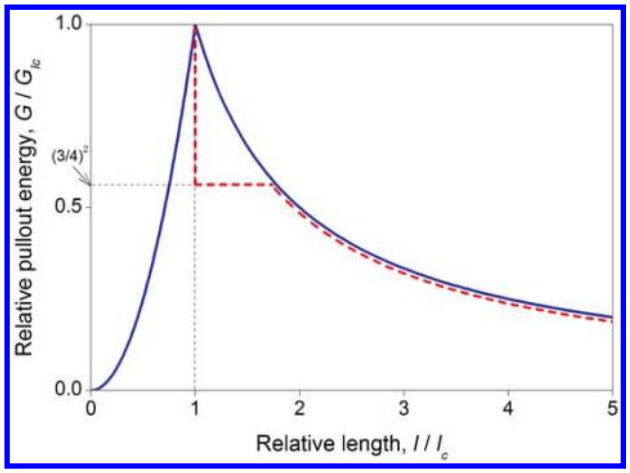

Figure 9 Universal curve depicting relative pullout energy G/G_{lc} versus relative filler length l/l_c (equation (22)): holds for any cross-sectional shape; dashed curve illustrates case of fillers somewhat longer than l_c described in text

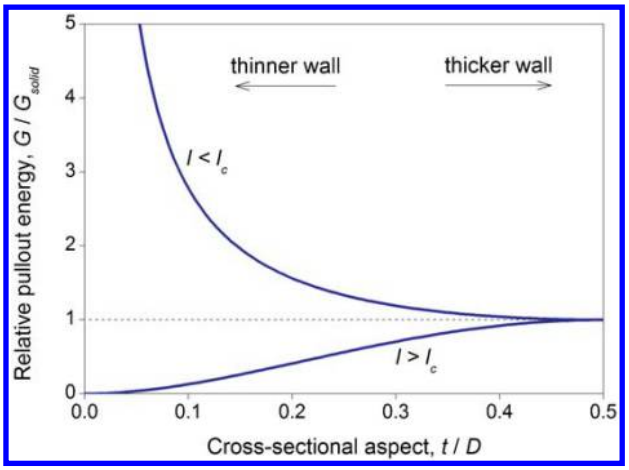

Figure 10 Dependence of relative pullout energy G/G_{solid} on cross-sectional aspect ratio t/D of circular hollow tube, when tube length l is longer (lower curve) and shorter (upper curve) than critical length l_c (equation (23) combined with equation (5)): maximum achievable G in domain $l<l_c$ is bounded by minimal possible wall thickness, and so long as l_c is not reduced below l

Combining the two length domains (equations (13) and (16)), and the maximum achievable pullout energy G_{lc} defined by equation (19), we obtain

$$G=\frac{V_f\sigma_f}{12}\begin{cases} l^2/l_c \\ l_c^2/l \end{cases}=G_{lc}\begin{cases} (l/l_c)^2, & l<l_c \\ (l/l_c)^{-1}, & l>l_c \end{cases} \tag{22}$$

which holds for any cross-sectional shape. So, the pullout energy when $l>l_c$ is higher for longer l_c and shorter l. By contrast, when $l<l_c$, the pullout energy is higher for shorter l_c and longer l. A universal pullout energy curve, obtained by normalizing G by G_{lc}, is depicted in Fig. 9.

Cottrell[15] points out an additional domain, where the filler length is longer than its critical length but not much longer. In the domain $l\gg l_c$, when a filler breaks, the nearby fillers will become overloaded and will also break, and therefore the crack will propagate at a cross-sectional plane. However, when $l>l_c$ (only slightly longer), the filler will not tend to break at the fracture plane but rather at its highly stressed length center, creating a 'new' composite with filler fragments of length $1/2\ l_c<l<l_c$ (fragments longer than l_c will rebreak). The pullout energy that corresponds to this case is given by equation (13), and will remain constant upon increasing the filler length (since the length remains constant on average after fragmentation), until, when $l\gg l_c$, it will gradually drop in accordance with equation (16). See illustration in Fig. 9.

Since the average fragment length in this domain is $l=3/4\ l_c$, the pullout energy will be, according to equation (13), lower by a factor of $(3/4)^2\cong 0.56$ compared to a filler that is slightly shorter than its critical length, or $l\cong l_c$. From a toughness perspective, since the pullout energy decreases from its peak for any filler length in the range $l>l_c$, whether somewhat longer or much longer than l_c, it is always preferable to use fillers that are slightly shorter than their l_c.

The effect of the aspect ratio t/D of a circular hollow tube can be summarized from equations (15) and (18)

$$G=G_{solid}\begin{cases} A_{tD}^{-1}, & l<l_c \\ A_{tD}^{2}, & l>l_c \end{cases} \tag{23}$$

depicted in Fig. 10. So, when $l>l_c$, the higher the aspect ratio (thicker tube wall), the higher the pullout energy. In other words, hollow tubes in this domain dissipate less pullout energy compared to solid fibers. By contrast, when $l<l_c$, the lower the aspect ratio (thinner tube wall), the higher the pullout energy. In other words, hollow tubes in this domain dissipate more pullout energy than solid fibers, and more so at lower values of the aspect t/D (i.e. shorter l_c according to equation (7)). We can keep on reducing t/D in order to increase the pullout energy, so long as l_c does not become smaller than l, switching to the domain $l>l_c$. Clearly, the wall thickness cannot be reduced below the width of a single layer of atoms as in a single wall nanotube.

The combined effect of the diameter and aspect ratio for a circular hollow tube can be expressed by rewriting equation (22) in the following form

$$G=G_{max}\begin{cases} (l_c/l)^{-1}, & l<l_c \\ (l_c/l)^2, & l>l_c \end{cases} \tag{24}$$

where l_c is given in equation (7), and the term $G_{max}=V_f\sigma_f l/12$ indicates the maximum possible pullout energy that can be achieved for a given tube length l by matching l_c to it. When $l\ll l_c$ (Fig. 11) as is typical for most current nanotubes, the effect of reducing the diameter at a given tube length has a dramatic positive impact on the pullout energy. This size effect occurs earlier (i.e. at a larger diameter) for lower aspect ratios (thinner wall thickness). In other words, the maximum pullout energy for a given tube length can be achieved by gradually reducing the external diameter, while preferably keeping a thin wall, effectively diminishing the critical length toward the tube length. If the diameter is reduced beyond the point where $l=l_c$, the trend will be reversed and the pullout energy will gradually decrease.

Effect of filler shape on strength and stiffness

A change in a design parameter, such as the filler's length or cross-sectional shape, in order to improve one material

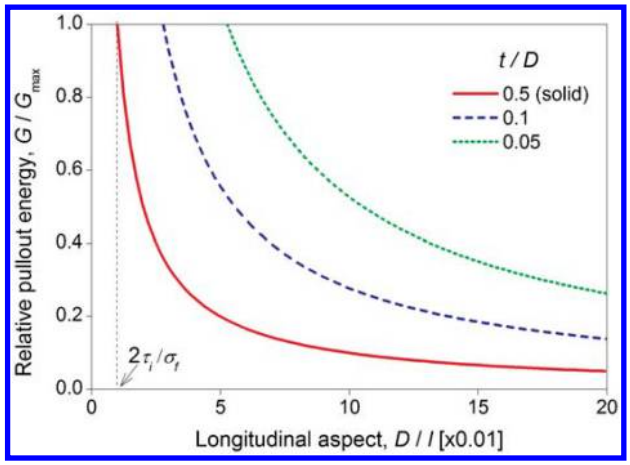

Figure 11 Relative pullout energy G/G_{max} versus longitudinal aspect ratio D/l for three aspect ratios t/D of circular hollow tube (equation (24) combined with equation (7)): plotted for domain $l<l_c$, with $2\tau_i/\sigma_f=0.01$

property, does not necessarily result in improving the other. Specifically, we are interested in studying the tradeoffs between the composite strength, stiffness and toughness, with respect to the filler geometry. We now use existing composites strength and stiffness models (for an example see Ref. 17) and generalize them to an arbitrarily shaped hollow filler. We then compare their strength and stiffness parametric trends to those of the toughness model.

Composite strength

Consider a composite's RVE, whose total cross-sectional area is A. The matrix has an ultimate strength σ_m, containing evenly dispersed unidirectional filler with ultimate strength σ_f. The filler is a general cylinder with length l, material cross-section area a and perimeter p (Fig. 2). When a sufficiently high load is applied on the composite, the interfacial stress is assumed to reach a constant value τ_i as previously described, corresponding to the matrix yield strength or the interfacial bonding strength. The stress in the filler, as a function of the distance x from the filler end, can be derived by substituting the ratio p/a from equation (3) into equation (2)

$$\sigma(x)=\tau_i x\frac{p}{a}=\frac{2\sigma_f x}{l_c},\ \ \sigma(x)\le\sigma_f \tag{25}$$

Note that this formulation is universal with respect to the filler's cross-sectional shape and lateral size. At distances longer than $l_c/2$ from the filler end, the filler stress will reach its ultimate strength σ_f.

When an ultimate load F is applied, a crack develops in the matrix as a result of small debonding cracks at the filler ends. Consequently, fillers that are embedded a short length beyond the fracture plane will pull out, while those that are embedded longer will break at the fracture plane. So, except for shortly embedded filler sections, both matrix and filler are simultaneously exploited to their ultimate strength. The force borne by the matrix surface bonded to the filler end is neglected, since it is much lower than the pullout force.

When the filler length is shorter than its critical length $l<l_c$, the maximum stress in the filler occurs at $x=l/2$, where $\sigma(l/2)<\sigma_f$, and the filler's contribution to the overall stress is by means of pullout. Since the matrix fracture plane can fall anywhere between the filler ends, the average stress in the filler at the fracture surface is $1/2\ \sigma(l/2)$, and the longitudinal strength of the composite is

$$\begin{aligned}\sigma_c&=\frac{F}{A}=\frac{F_{filler}^{pullout}+F_{matrix}^{ultimate}}{A}\\&=1/2\frac{Na}{A}\sigma(l/2)+\frac{A_{matrix}}{A}\sigma_m,\ \ l<l_c\end{aligned} \tag{26}$$

where N is the average number of fillers intersecting the fracture surface, and A_{matrix} is the material cross-sectional area of the matrix. Using N from equation (10) and $\sigma(l/2)=\sigma_f l/l_c$ from equation (25)

$$\sigma_c=1/2\frac{l}{l_c}V_f\sigma_f+V_m\sigma_m,\ \ l<l_c \tag{27}$$

where V_f and V_m are the filler and matrix volume fractions, respectively. Note that V_m is slightly less than $(1-V_f)$ for hollow fillers (see more on this further on). This equation is invariant with respect to the cross-sectional shape and lateral size, in other words it is a generalization of standard fiber reinforcement models such as in Ref. 17 to arbitrarily shaped fillers. As for the pullout energy in this length domain, a higher l/l_c improves the composite strength. Furthermore, the same value of the maximum composite strength can be achieved either by increasing l toward l_c or decreasing l_c toward l, contrary to the maximum pullout energy (G_{Ic} from equation (19)), which decreases when l_c is decreased. The maximum contribution of the filler to the composite strength is $1/2V_f\sigma_f$.

For a thin wall hollow filler with a wall thickness t, we substitute l_c from equation (4)

$$\sigma_c^{thin}\cong 1/4\frac{\tau_i}{\sigma_f}\frac{l}{t}V_f\sigma_f+V_m\sigma_m,\ \ l<l_c \tag{28}$$

independent of the cross-section shape and lateral size. In the case of a thin wall ribbon shaped filler (e.g. graphene), the contribution of the filler to the composite strength will improve by a factor of 2 as a result of the duplication of the interfacial area, as for the pullout energy in this length domain.

For a circular hollow tube, we substitute l_c from equation (7)

$$\sigma_c=\left(\frac{\tau_i}{\sigma_f}\frac{l}{D}A_{tD}^{-1}\right)V_f\sigma_f+V_m\sigma_m,\ \ l<l_c \tag{29}$$

depicted in Figs. 13 and 14. For a solid fiber, substitute $A_{tD}=1$. Note that σ_f can be eliminated from equations (28) and (29) (it appears in both the numerator and denominator), since the filler ultimate strength is not reached in the domain $l<l_c$.

When the filler length is longer than its critical length $l>l_c$, at a distance longer than $l_c/2$ from the filler ends the fracture stress is σ_f for a fraction of $(l-l_c)/l$ of the fillers, while at shorter distances from the ends the filler's contribution to the overall stress is through pullout and its average stress is $1/2\ \sigma_f$ for a fraction of l_c/l of the fillers. Thus, the composite longitudinal strength is

$$\begin{aligned}\sigma_c&=\frac{F}{A}=\frac{F_{filler}^{pullout}+F_{filler}^{ultimate}+F_{matrix}^{ultimate}}{A}\\&=1/2\frac{Na}{A}\frac{l_c}{l}\sigma_f+\frac{Na}{A}\frac{l-l_c}{l}\sigma_f+\frac{A_{matrix}}{A}\sigma_m,\ \ l>l_c\end{aligned} \tag{30}$$

Using N from equation (10)

$$\sigma_c = \left(1 - 1/2\frac{l_c}{l}\right) V_f\sigma_f + V_m\sigma_m,\ \ l > l_c \tag{31}$$

invariant with respect to the cross-sectional shape and lateral size. Note that, contrary to the pullout energy in this length domain, a higher l/l_c improves the composite strength, and the maximum strength is obtained for long fillers ($l \gg l_c$), for which equation (31) reduces to the known mixture rule, $\sigma_c = V_f\sigma_f + V_m\sigma_m$. Thus, the maximum contribution of the filler to the composite strength is $V_f\sigma_f$, while the minimum is $1/2V_f\sigma_f$.

For a thin wall hollow filler with a wall thickness t, we substitute l_c from equation (4)

$$\sigma_c^{thin} \cong \left(1 - \frac{\sigma_f}{\tau_i}\frac{t}{l}\right) V_f\sigma_f + V_m\sigma_m,\ \ l > l_c \tag{32}$$

independent of the cross-section shape and lateral size. For a very thin filler wall (small t), this equation reduces to the same simple mixture rule as for very long fillers, implying that for a given volume fraction, a short hollow filler can deliver the same composite strength as a long solid filler, while maintaining toughness by keeping its length slightly below the critical length. We elaborate on such length-thickness tradeoffs further on. In the case of a thin wall ribbon-shaped filler (e.g. graphene), the contribution of the filler to the composite strength will improve (by a factor smaller than 2) as a result of the duplication of the interfacial area, contrary to the pullout energy in this length domain.

For a circular hollow tube, we substitute l_c from equation (7)

$$\sigma_c = \left(1 - 1/4\frac{\sigma_f}{\tau_i}\frac{D}{l}A_{tD}\right) V_f\sigma_f + V_m\sigma_m,\ \ l > l_c \tag{33}$$

depicted in Figs. 13 and 14. For a solid fiber, substitute $A_{tD}=1$. Note that reducing the cross-section aspect t/D (lower A_{tD}) has the same effect on improving the composite strength as reducing the longitudinal aspect D/l.

As mentioned before, V_m is slightly lower than $(1-V_f)$ when the filler contains cavities. Thus, a correction factor is needed for hollow fillers if the matrix material (e.g. polymer) does not penetrate the filler's cavities, particularly when the longitudinal aspect ratio l/D is high or when the internal cavity is narrow or closed at its ends (e.g. in CNT). In such cases, the filler cavities are void and do not share the load. Thus, using equations (5) and (10)

$$V_m = 1 - \frac{Na_{tot}}{A} = 1 - \frac{V_f}{A_{tD}} \tag{34}$$

where a_{tot} is the total area bounded by the filler perimeter p, and the term on the right is for a circular hollow tube. Consequently, for a given volume fraction, while a thinner tube wall (smaller A_{tD}) improves the contribution of the filler to the composite's strength, it weakens the contribution of the matrix. Similarly, V_m should also be corrected for gaps between closely-packed fillers, which are not penetrated by the matrix or are too small to share the load, as in the case of NT bundles (Appendix).

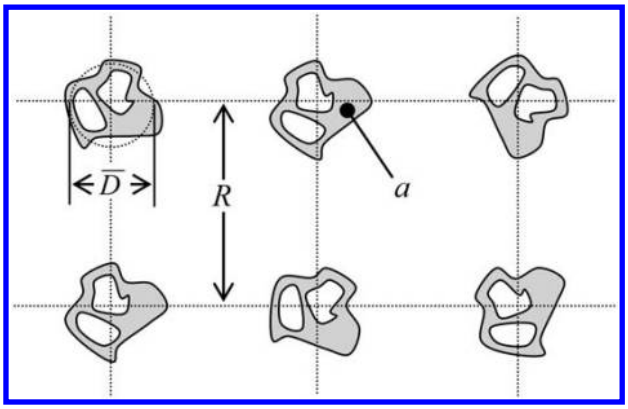

Figure 12 Square packing of hollow fillers with arbitrarily shaped cross-section: *R* is mean distance between fillers, *a* is filler material cross-section area and $\bar{D}$ is filler mean lateral size

Composite stiffness

The theoretical model for the elastic modulus of a composite with unidirectional reinforcing fibers was developed by Cox, using the shear lag theory.[17,20] We adjust the model for a filler with an arbitrarily shaped cross-section

$$E_c = \left[1 - \frac{\tanh(\beta l/2)}{\beta l/2}\right] V_f E_f + V_m E_m,\ \ \beta^2 = \frac{2\pi G_m}{E_f a \ln(2R/\bar{D})} \tag{35}$$

where E_f and E_m are the tensile moduli of the filler and the matrix respectively, G_m is the matrix shear modulus, a is the filler material cross-section area, $\bar{D}$ is the filler mean lateral dimension and R is the mean lateral distance between adjacent fillers (Fig. 12). As in the strength model, V_m is slightly less than $(1-V_f)$ for slender hollow fillers, as calculated by equation (34).

Note that R is a mean value for the distance between fillers that protrude through an arbitrary cross-section of the composite. Assuming square lateral packing, a single cell $R \times R$ has an area R^2, and contains four portions of a filler with an average cumulative area a. Hence, the filler volume fraction is $V_f = a/R^2$, and therefore

$$\ln\left(\frac{2R}{\bar{D}}\right) = 1/2\ln\left(\frac{4a}{V_f\bar{D}^2}\right) \tag{36}$$

Contrary to the pullout energy, when extending the length of the filler (very large l), the bracketed term in equation (35) has an upper limit value of 1, and the composite's elastic modulus reaches its maximum (for a given volume fraction), expressed by the known mixture rule, $E_c = V_f E_f + V_m E_m$. Thus, the maximum contribution of the filler to the composite stiffness is $V_f E_f$.

For a thin wall hollow filler with a wall thickness t, we approximate the filler perimeter by $\pi\bar{D}$, and therefore the cross-section material area can be estimated by $a \cong \pi\bar{D}t$. Substituting into equation (35) and using equation (36), we arrive after rearrangement of terms at the following estimation

$$\left(\frac{\beta l}{2}\right)_{thin} \cong \frac{l}{\bar{D}}\left(\frac{G_m}{E_f}\right)^{1/2}\left[\frac{t}{\bar{D}}\ln\left(\frac{4\pi}{V_f}\frac{t}{\bar{D}}\right)\right]^{-1/2} \tag{37}$$

Note that, unlike the toughness and strength, the stiffness of a thin wall filler is dependent on the cross-section mean

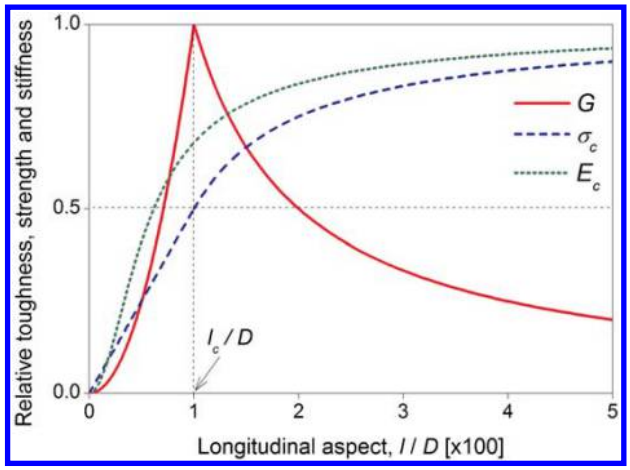

Figure 13 Relative toughness G/G_{lc} (equation (22) combined with equation (7)), strength $\sigma_c/(V_f\sigma_f)$ (equations (29) and (33)) and stiffness (elastic modulus) $E_c/(V_fE_f)$ (equations (35) and (39)) versus longitudinal aspect ratio l/D of circular hollow tube: toughness and strength curves are plotted for $l_c/D=\sigma_f A_{tD}/(2\tau_i)=100$; thinner wall tube will shift l_c/D point to left (i.e. aspect function A_{tD} will be smaller, *see* equation (5)); stiffness curve is plotted for $G_m/E_f=10^{-3}$ and $A_{tD}\ln(\pi A_{tD}/V_f)=4$; thinner wall tube will stretch graph upward; strength and stiffness curves account only for filler's contribution to composite (first term in equations (29), (33) and (35))

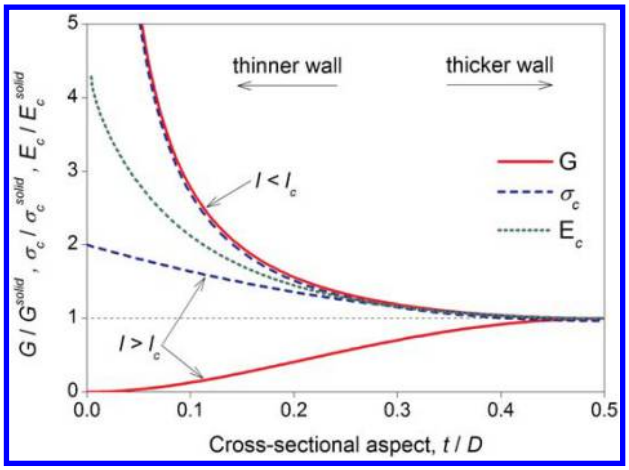

Figure 14 Relative toughness G/G^{solid} (equation (23)), strength $\sigma_c/\sigma_c^{solid}$ (equations (29) and (33)) and stiffness E_c/E_c^{solid} (equations (35) and (39)) versus cross-sectional aspect ratio t/D of circular hollow tube: aspect function A_{tD} is given by equation (5), and is equal to 1 for solid fiber; strength curve for $l>l_c$ is plotted for $l/l_c^{solid}=2(l/D)(\tau_i/\sigma_f)=1$; higher values will squeeze graph downward, with minimum at 1; lower values will stretch it upward, with maximum at the $l<l_c$ curve; stiffness curve is plotted for $(l/D)(G_m/E_f)^{1/2}=1$ and $V_f=0.05$; higher values will squeeze graph downward (with minimum at 1), while lower values will stretch it upward; strength and stiffness curves account only for filler's contribution to composite (first term in equations (29), (33) and (35))

size $\overline{D}$, which appears in the longitudinal and cross-sectional mean aspect ratios, $l/\overline{D}$ and $t/\overline{D}$ respectively. For a very thin filler wall (small values of $t/\overline{D}$), the term $\beta l/2$ of equation (37) becomes very large, and equation (35) reduces to the same simple mixture rule as for very long fillers. This outcome implies that, for a given volume fraction, a short hollow filler can deliver the same composite stiffness as a long solid filler, without compromising the toughness if its length is kept slightly below the critical length. More on such tradeoffs is discussed further on.

In the case of a circular hollow tube, we replace (with the help of equation (5)) $\overline{D}=D$ and $a=\pi D^2 A_{tD}/4$, thus

$$\ln\left(\frac{2R}{\overline{D}}\right)=\frac{1}{2}\ln\left(\frac{\pi A_{tD}}{V_f}\right) \tag{38}$$

Substituting into equation (35)

$$\frac{\beta l}{2}=2\frac{l}{D}\left(\frac{G_m}{E_f}\right)^{1/2}\left[A_{tD}\ln\left(\frac{\pi A_{tD}}{V_f}\right)\right]^{-1/2} \tag{39}$$

which reduces to the known expression for a solid fiber when $A_{tD}=1$. Equation (35) with equation (39) is depicted in Figs. 13 and 14. Note that reducing the cross-section aspect t/D (lower A_{tD}) has the same effect on improving the composite stiffness as increasing the longitudinal aspect l/D. When the cross-section aspect is increased (higher A_{tD}), the composite's elastic modulus monotonically diminishes until it reaches a minimum at a solid fiber. Hence, when high stiffness is desired (at a given volume fraction), a thin wall filler is preferable to a solid fiber.

Comparison to toughness

Reinforcement design is the result of a tradeoff between the desired composite performance criteria, mainly its toughness, strength, and stiffness (elastic modulus), which are determined by the filler's length, cross-sectional shape, mechanical properties and volume fraction, as well as by the matrix and interface mechanical properties. The following description highlights some of these dependencies, for a fixed filler volume fraction.

The plot in Fig. 13 summarizes the composite's toughness, strength and stiffness performance as a function of the longitudinal aspect ratio l/D of a circular hollow tube. In the domain $l<l_c$, a common case for nanoreinforcement, the performance parameters improve simultaneously when the ratio l/l_c is increased, either by increasing l or decreasing l_c. By contrast, in the domain $l>l_c$, a typical case for microreinforcement, when the strength and stiffness improve, the toughness degrades. However, the strength and stiffness in the domain $l<l_c$ are much lower compared to the domain $l>l_c$, and do not approach their optimal values. For example, when the toughness is at its optimum ($l=l_c$), the composite strength is only half its maximum possible value.

Furthermore, when $l\ll l_c$ as is typical for nanotubes, reducing the diameter has a dramatic positive impact on all three performance parameters. By gradually reducing the external diameter, the toughness increases toward its maximum value, while the strength and stiffness increase as well. This size effect occurs earlier for lower aspect ratios (thinner wall thickness). However, when $l>l_c$, the toughness trend with respect to the diameter is reversed, while the strength and stiffness keep improving.

The effect of the cross-sectional aspect ratio t/D of a circular hollow tube is depicted in Fig. 14. In the domain $l<l_c$, the performance parameters improve simultaneously

when t/D is decreased (thinner tube wall). By contrast, in the domain $l>l_c$, when the strength and stiffness improve, the toughness degrades. When the tube's longitudinal aspect ratio l/D is increased to high values, the strength and stiffness level off (Fig. 13) at a maximum value, and cannot be further improved by modifying the cross-sectional aspect ratio.

Geometric tradeoffs

We observe that the equations describing the composite toughness (equations (15) and (18)), strength (equations (29) and (33)) and stiffness (equations (35) and (39)) for circular hollow fillers contain functions of both the longitudinal aspect l/D and the cross-sectional aspect t/D, whereas the common models for circular solid fillers (e.g. fibers) contain l/D only. Hence, where hollow fillers are concerned, both geometrical aspect ratios play a significant role in determining the overall mechanical performance of the composite. In fact, the overall performance is the result of a tradeoff between the two aspect ratios, which can be visualized by writing equal performance expressions for G, σ_c and E_c, based on the aforementioned equations

$$\left.\begin{array}{l}(l^2/D)_G^{l<l_c}\\ (l^{1/2}/D)_G^{l>l_c}\\ (l/D)_{\sigma c}\end{array}\right\}\sim A_{tD}$$
$$(l/D)_{Ec}\sim[A_{tD}\ \ln(\pi\ A_{tD}/V_f)]^{1/2} \quad (40)$$

where A_{tD} is the aspect function of t/D defined in equation (5). The dependencies in equation (40), depicted in Fig. 15, were derived by expressing l/D as functions of t/D, where all other parameters are assumed constant. Although, in the case of G, the longitudinal aspect is expressed as l^2/D ($l<l_c$) and $l^{1/2}/D$ ($l>l_c$), the trend of l/D is maintained and it acts in the same direction for both l domains.

Figure 15 demonstrates the performance invariance with respect to size scaling (e.g. from microscale to nanoscale, and *vice versa*) obtained by modulating the geometric parameters D, t and l. It can be seen, for all three performance parameters, that the longitudinal aspects l^n/D are monotonically increasing functions of t/D. Consequently, a desired performance change obtained by increasing (or decreasing) l/D can be matched by increasing (or decreasing) t/D instead, of course within the minimum and maximum wall thickness boundaries. This means, for example, that the overall performance of short hollow fillers, typical of nanofillers, can match and even exceed that of long solid microfillers. In the case of G, t/D can be decreased so long as the resulting G_{Ic} (equation (21)) does not drop below the desired G.

The following example, comparing the composite strength of two alternative fillers with the same tensile and interfacial strength and same volume fraction, but with a completely different size scale, may help clarify the issue. First, consider a solid fiber with $D=1$ μm and $l=1$ mm, which delivers a desired composite strength. Its aspect ratios are $t/D=0.5$ and $l/D=1000$, denoted by point F on Fig. 15 (l/D is normalized to 1). Now, exchange this filler by a hollow single wall nanotube, with $D=20$ nm and $t=0.34$ nm, so that $t/D=0.017$. Its corresponding length is $l=1.3$ μm ($l/D=67$),

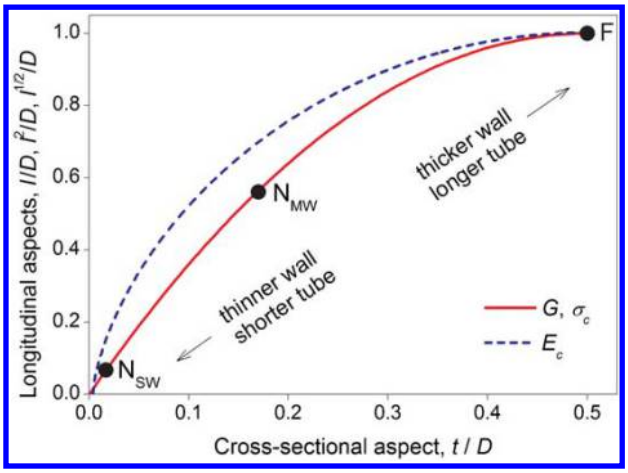

Figure 15 Equal composite performance curves (or lines of isoperformance) of the toughness G, strength σ_c and stiffness E_c, depicted in aspect ratios space – longitudinal aspect l^n/D versus cross-sectional aspect t/D, for a circular hollow tube (equation (40)): longitudinal aspects are l/D for σ_c and E_c, l^2/D for G when $l<l_c$, and $l^{1/2}/D$ for G when $l>l_c$, normalized to a maximum value 1; E_c curve is plotted for $V_f=0.05$; points F, N_{MW} and N_{SW} denote solid fiber, multiwall nanotube and single wall nanotube examples respectively, discussed in the text

denoted by point N_{SW} in Fig. 15. Optionally, we exchange the filler by a multiwall nanotube, with $D=20$ nm and $t=3.4$ nm (10 single atom layers), so that $t/D=0.17$ and $l=11.3$ μm ($l/D=560$), denoted by point N_{MW} in Fig. 15. All three filler types deliver the same composite strength (however, since nanotubes are typically stronger than fibers, they will in fact deliver higher composite strength, as discussed in the next section). Similar calculations, carried out for the toughness and stiffness using equation (40) and Fig. 15, show similar geometrical tradeoffs.

Nanotoughness compared to microtoughness

The potential toughness, strength and stiffness performance of nanoreinforcement using multiwall CNT fillers, is compared to microreinforcement using carbon microfibers (CFs), expanding our previous work.[10,13] We focus on the following four types of gedanken experiments illustrated in Figure 16*b–e*, compared to the reference carbon microfiber configuration in Fig. 16*a*, assuming the same filler volume fraction for both nanotubes and microfibers.

First, we consider uniformly dispersed unidirectional long carbon nanotubes, of length $l=l_c$ (Fig. 16*c*), a somewhat optimistic assumption in view of current technological feasibility. The length of the reference carbon microfibers is assumed to be $l=l_c$ as well. Using the optimal pullout energy $G_{Ic}=V_f\sigma_f^2D/(24\tau_i)$ from equation (21), the toughness performance ratio between CNT and CF reinforced composites is estimated by

$$\frac{G_{NT}}{G_{CF}}=\frac{G_{IcNT}}{G_{IcCF}}=\frac{\sigma_{NT}^2D_{NT}\tau_{iCF}}{\sigma_{CF}^2D_{CF}\tau_{iNT}}\approx\left(\frac{\sigma_{NT}}{\sigma_{CF}}\right)^2\frac{D_{NT}}{D_{CF}}\sim 1 \quad (41)$$

assuming the same interfacial strength for both filler types, $\tau_{iCF}\cong\tau_{iNT}$. In this equation, the following order of magnitude

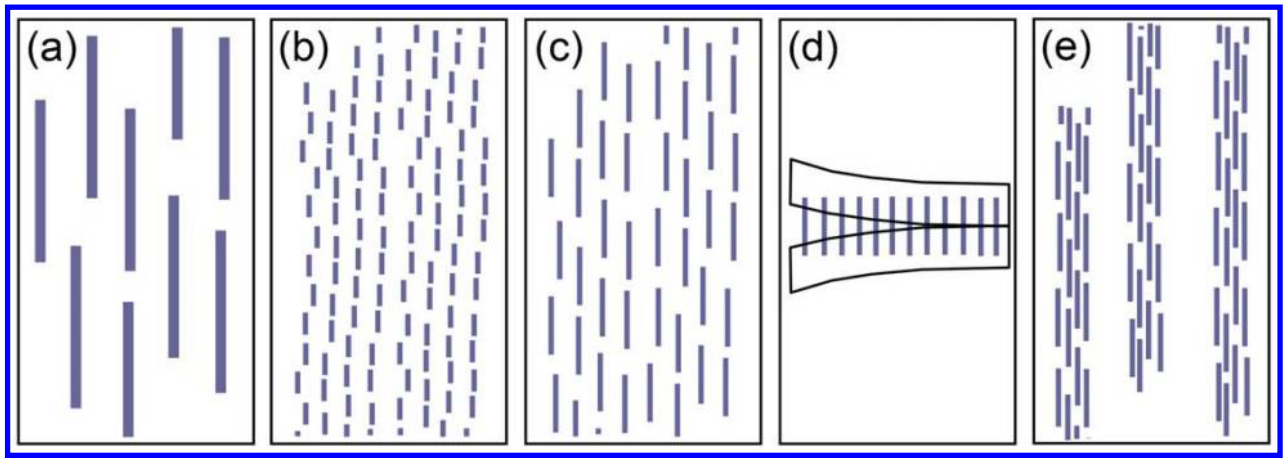

Figure 16 Gedanken experiments of unidirectionally aligned nanoreinforcing fillers: *a* uniformly dispersed long CF (reference configuration); *b* uniformly dispersed short NT; *c* uniformly dispersed long NT; *d* interlaminar reinforcement by long NT; *e* uniformly dispersed long NT fibers (NTF)

ratios were used: $\sigma_{NT}/\sigma_{CF}\sim 10$ and $D_{NT}/D_{CF}\sim 0.01$. This estimate finds the microfibers and nanotubes equivalent in their composite toughness. Note that the use of graphene has the potential of improving the nanoreinforcement by a factor of 2. The strength and stiffness performance ratios for this structure are estimated by $\sigma_{NT}/\sigma_{CF}\sim 10$ (equation (27)) and $E_{NT}/E_{CF}\sim 10$ (equation (35)) respectively, demonstrating a potential advantage for the nanotube reinforced composite, even though the toughness is not improved.

As already noted, most current CNTs are shorter than their critical length, and therefore for such cases the assumption $l=l_c$ used in the previous structure (equation (41)) should be replaced by $l<l_c$ (Fig. 16*b*)). Using a nanotube length of order $l_{NT}/l_{cNT}\approx 0.1$ for this structure, the toughness ratio estimate is reduced by the factor $(l_{NT}/l_{cNT})^2\sim 0.01$ (equation (22)) with respect to equation (41), favoring microfibers over nanotubes. If, however, we use single wall instead of multiwall nanotubes, the critical length can possibly be reduced so that $l_{NT}/l_{cNT}\approx 1$, and consequently, the toughness will decrease (in accordance with equation (21)) only by the factor $A_{tD}\sim 0.1$ (assuming $t/D\approx 0.025$)

$$\frac{G_{NT}}{G_{CF}}=\frac{G_{lcNT}^{thin}}{G_{lcCF}}=\frac{G_{lcNT}^{solid}}{G_{lcCF}}A_{tD}\sim 0.1 \tag{42}$$

where we used $G_{lcNT}^{solid}/G_{lcCF}\sim 1$ from equation (41). The strength and stiffness performance ratio for this structure are estimated by $\sigma_{NT}/\sigma_{CF}\sim 10$ (equation (27)) and $E_{NT}/E_{CF}\sim 10$ (equation (35)) respectively, demonstrating a potential advantage for the nanotube reinforced composite, even though the toughness is degraded.

A compact nanotubes packing was demonstrated by Garcia *et al.*,[22] using reinforcement by a forest of aligned carbon nanotubes transplanted in the interlaminar region in laminates (Fig. 16*d*). Analysis of a similar structure was carried out by Wagner et al.,[13,14] considering a large number of parallel nanotubes with their total volume equivalent to that of a microfiber, yielding

$$\frac{nG_{NT}}{G_{CF}}=\frac{nD_{NT}\tau_{iNT}l_{cNT}^2}{D_{CF}\tau_{iCF}l_{cCF}^2}\approx\frac{\sigma_{NT}}{\sigma_{CF}}\sim 10 \tag{43}$$

where $n=(D_{CF}^2/D_{NT}^2)(l_{cCF}/l_{cNT})$ is the number of nanotubes, and assuming $l=l_c$ for both the nanotubes and the microfiber. This structure is advantageous to nanotubes. The strength performance ratio for this structure is estimated by $(\sigma_{NT}/\sigma_{CF})(l_{cCF}/l_{cNT})\cong D_{CF}/D_{NT}\sim 100$, demonstrating a significant potential advantage for the nanotube reinforced composite, as well as toughness improvement.

The fourth structure compared here is a composite reinforced by long bundles of aligned compactly packed carbon nanotubes, or nanotube fibers (NTFs) (Fig. 16*e*), discussed in Appendix. The toughness performance ratio is (equations (49) and (21))

$$\frac{G_{NTF}}{G_{CF}}=\frac{G_{lcNTF}}{G_{lcCF}}\approx\left(\frac{\sigma_{NT}}{\sigma_{CF}}\right)^2\frac{D_{NTF}}{D_{CF}}\approx\left(\frac{\sigma_{NT}}{\sigma_{CF}}\right)^2\sim 100 \tag{44}$$

using $D_{NTF}/D_{CF}\sim 1$, and assuming $l=l_c$ for both the nanotube fibers and the carbon fibers. This structure offers a substantial potential advantage over carbon microfibers. The strength and stiffness performance ratios for this structure are estimated by $\sigma_{NT}/\sigma_{CF}\sim 10$ (equation (27)) and $E_{NT}/E_{CF}\sim 10$ (equation (35)) respectively, advantageous as well to the nanotube fibers. These estimates suppose perfect compact packing of the nanotubes in each bundle, and efficient stress transfer from the bundle's boundary to its core, both somewhat compromised in practice due to gaps between the nanotubes and matrix penetration into the bundle (Appendix).

Based on the above estimates, the relative toughness, strength and stiffness of the four nanostructural types of Fig. 16*b–e*, with respect to the reference carbon microfiber configuration of Fig. 16*a*, are illustrated in Fig. 17. From a mechanical viewpoint, the nanocomposite structures of Fig. 16*c–e* are most advantageous, showing a potential simultaneous improvement in toughness, strength and stiffness.

As a final comment, we address the potential performance of composites reinforced by inorganic nanotubes such as WSNTs. Recent studies[23,24] have shown that, although WSNTs are intrinsically weaker than CNTs, WSNT reinforced composites have a comparable and sometimes higher toughness compared to CNT reinforced composites, without compromising other mechanical properties. Among the reasons cited in these studies is the presence of sulfide and oxysulfide functional groups, which increases the

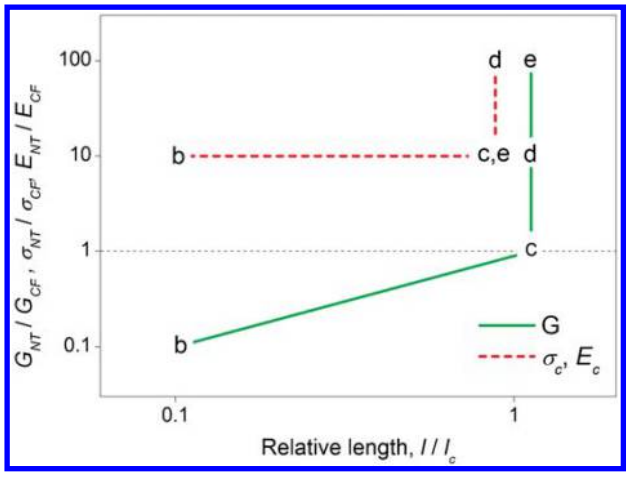

Figure 17 Nanoreinforcement potential – carbon nanotubes (NTs) compared to carbon microfibers (CFs): relative toughness G_{NT}/G_{CF}, strength σ_{NT}/σ_{CF} and stiffness E_{NT}/E_{CF}, versus relative length l/l_c; letters refer to structural types defined in Fig. 16

cross-linking within the matrix and the interfacial strength between the WSNTs and the matrix, and generates a more uniform and controlled dispersion of the WSNTs in the matrix, in contrast to the tendency of CNTs to aggregate. These preliminary results should be substantiated and expanded, for example by means of experimental data on the interfacial strength between WSNTs and various matrix materials.

Conclusion

The present analysis generalizes the modeling of the mechanical properties of composites comprising a soft matrix and unidirectional uniformly dispersed hollow fillers with arbitrarily shaped cross-sections, typical of nanoreinforced composites. The generalized model applies to a wide variety of filler types, including CNT, WSNT, MSNP and CNT fibers (CNTF). Of particular interest in this work is the evaluation of the composite toughness, strength and stiffness dependence on the filler size and shape characteristics, such as diameter, wall thickness and length. The toughness was expressed by the energy dissipated when the filler pulls out from the matrix during the composite fracture, taking into consideration the filler critical length.

It is shown that the critical length and the pullout energy of a thin wall filler, such as a single wall carbon nanotube (SWCNT), depend on the wall thickness rather than on the external shape and lateral size of the filler. This outcome leads to an analogy between a thin wall filler and a thin flat ribbon such as graphene, which has a double sided bonding area and hence half the critical length. The use of graphene instead of nanotubes may therefore offer improvement of the composite toughness in those cases where a shorter critical length is desired.

A convenient function of the aspect ratio between the wall thickness and the outer diameter is used to express the effect of the wall thickness on the critical length and pullout energy of hollow tubes. This function, termed the 'aspect function', rises monotonically with the aspect ratio (from a thin wall tube to a solid fiber). A tradeoff exists between the filler cross-sectional aspect ratio (wall thickness/diameter) and longitudinal aspect ratio (length/diameter), such that a desired performance can be achieved by modifying either of them. In this way, for example, thin wall short fillers can match the performance of long solid fillers at the same volume fraction.

Two filler length categories are characterized with respect to the filler critical length, regardless of the cross-sectional shape: fillers shorter than their critical length, whose pullout energy is inversely dependent on the critical length, and fillers longer than their critical length, whose pullout energy is proportional to the square of the critical length. The maximum pullout energy is achieved when the filler length is slightly below the critical length. Nanotubes typically belong to the short filler category, and therefore, to achieve a high pullout energy, their critical length should be shortened. This can be achieved by selecting nanotubes with smaller diameter and/or wall thickness (e.g. switching from MWCNT to SWCNT), keeping the filler volume fraction constant, as well as by increasing the interfacial strength (e.g. by using a stronger matrix or by functionalizing the nanotubes[11]). These dependencies reverse when the filler is longer than the critical length.

The parametric trends regarding the toughness of short fillers coincide with those for the composite strength and stiffness, such that decreasing the critical length benefits all. By contrast, in the domain of long fillers, the trends are reversed, and an increase in the critical length benefits the toughness while degrading the strength and stiffness, and vice versa.

Comparison of the reinforcement performance of CNT to carbon microfibers, when the filler is uniformly and unidirectionally dispersed in the matrix at the same volume fraction, shows that nanotubes have the potential of simultaneously achieving up to two orders of magnitude better toughness, strength and stiffness, depending on the structural configuration. Specifically, nanotubes are most advantageous when their length approaches their critical length, and when they are compactly packed in structures such as aligned forests embedded in the interlaminar region of laminates, or long woven bundles in the form of fibers (CNTF). An interesting outcome of the analysis is that aligned agglomerations of nanotubes that form bundles may be advantageous in toughness compared to unbundled nanotubes.

The full potential of nanocomposites is yet to be achieved. Challenges are still high in forming desired superstructures of nanofillers in the matrix, with the intention of exploiting their utmost properties. Current technology runs into difficulties in obtaining homogenous blends of nanotubes in a polymer solution, achieving unidirectional alignment of nanotubes in a matrix, or reaching a very high filler volume fraction as in biological tissues. However, the present analysis demonstrates how the properties of nanocomposites can be optimized by modulating the filler shape and dimensions, as well as material and interface properties. In future work, the analysis will be expanded to randomly oriented nanofillers.

Conflicts of Interest

The authors have no conflicts of interest to declare.

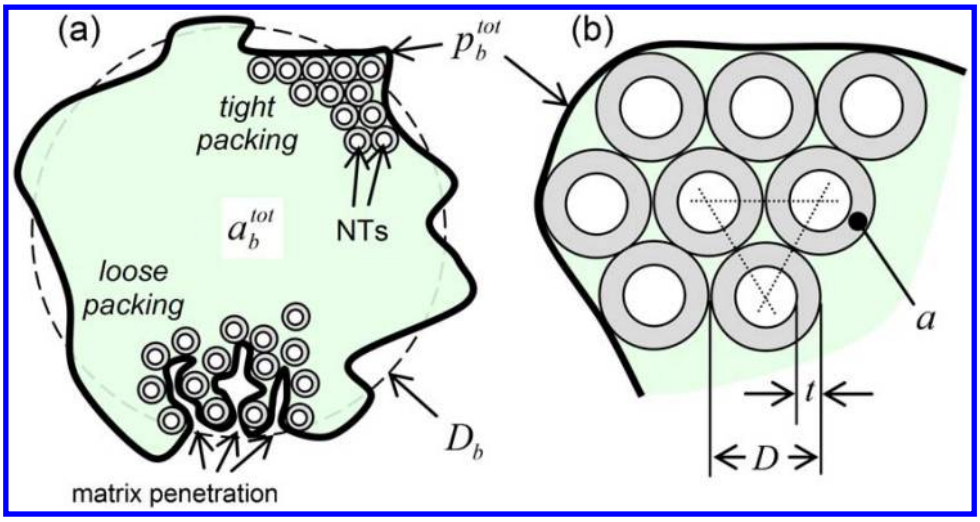

Figure A1 Cross-sectional view of nanotube bundle, illustrating *a* tight and loose packing and *b* magnified section of tight packing: *D*, *t* and *a* are diameter, wall thickness and material cross-sectional area of single NT respectively; p_b^{tot} is total outer perimeter of bundle, and a_b^{tot} is its total area (area bounded by perimeter p_b^{tot}); D_b is outer diameter of bundle with circular cross-section

Acknowledgements

The authors would like to acknowledge support from the INNI Focal Technology Area program 'Inorganic nanotubes (INT): from nanomechanics to improved nanocomposites', as well as from the G.M.J. Schmidt Minerva Centre of Supramolecular Architectures at the Weizmann Institute. This research was also made possible in part by the generosity of the Harold Perlman family. HDW is the recipient of the Livio Norzi Professorial Chair in Materials Science.

Appendix

Aligned nanotube bundles: example of complex geometry

Ultra long aligned CNT bundles, commonly termed CNT fibers or CNTF, synthesized by spray pyrolysis of ferrocene/xylene solutions, can reach several microns in diameter and contain 10^5–10^6 multiwall CNTs in a cross-section.[25,26] Within the same category of structures are bundles that contain a smaller amount of CNTs, which sometimes form spontaneously as a result of aligned agglomeration of CNTs in a polymer solution, for example under extensional flow.[3,4] The latter phenomenon is usually perceived as undesirable from a mechanical viewpoint, but this is not always the case as will be shown further on. The cross-sectional geometry of an aligned bundle is an example of a filler with arbitrarily shaped outline and multiple cavities, as presented in Fig. 1*a*. The following analysis applies the methods developed in this work to such bundles.

The calculation of the mechanical properties of aligned bundles embedded in a soft matrix should take into consideration the actual complex cross-sectional geometry of the bundle. Figure A1 illustrates the cross-section of a bundle for two types of packing: tightly packed nanotubes wherein the gaps between adjacent nanotubes are void of matrix material, and loosely packed nanotubes wherein the matrix material penetrates inside the bundle, thus increasing the effective interfacial area and affecting the stress transfer between outer and inner nanotubes.

Assuming the nanotubes in a bundle are tightly packed in a hexagonal array (Fig. A1*b*), the nanotube-matrix interface exists only at the external surface of the outermost nanotubes exposed to the matrix, and the stress in the bundle propagates inwards via interactions between adjacent nanotubes. Thus, the geometry is defined by the total outer perimeter of the bundle p_b^{tot} and the total area a_b^{tot} (the area bounded by the perimeter p_b^{tot}, including material and all forms of internal voids).

A correction factor should be applied to the perimeter, to account for the actual contact area between the matrix and the circular profile of each nanotube. For a nanotube with an external diameter *D*, the factor is equal to half its perimeter, $1/2\ \pi D$, divided by its width *D*, and therefore the actual perimeter is

$$p_b \cong \frac{1/2\pi D}{D} p_b^{tot} \cong \frac{\pi}{2} p_b^{tot} \tag{45}$$

Observing a representative area element indicated by a triangle in Fig. A1*b*, its material area fraction is equal to the material area of three 60° nanotube sections, $3/6a$ (*a* is the material cross-sectional area of a single nanotube), divided by the triangle area $3^{1/2}/4\ D^2$. Thus, the bundle material cross-sectional area is given by

$$a_b \cong \frac{1/2\ a}{3^{1/2}/4\ D^2} a_b^{tot} \cong \frac{\pi\ A_{tD}}{2 \times 3^{1/2}} a_b^{tot} \tag{46}$$

where A_{tD} is the cross-sectional aspect function of a single nanotube, defined in equation (5), which ranges from $4t/D \cong 0$ for a thin wall tube ($t \ll D$) to 1 for a solid fiber ($t = D/2$). If the nanotube wall thickness is unknown, the bundle's actual material cross-sectional area can be derived by $a_b = \rho_l/\rho_{NT}$, where ρ_l is the linear density of the bundle, and ρ_{NT} is the nanotube material density.

Substituting the bundle's actual perimeter p_b from equation (45) and its actual material cross-sectional area a_b from equation (46) into equation (3), we obtain the bundle's

critical length

$$l_{cb} = \frac{2\sigma_f}{\tau_i}\frac{a_b}{p_b} \cong \frac{2\sigma_f}{3^{1/2}\tau_i}\frac{A_{tD}}{p_b^{tot}} \quad (47)$$

regardless of the bundle cross-sectional shape. For a bundle with a circular cross-section having a diameter D_b (Fig. A1*a*), $a_b^{tot}/p_b^{tot} = \frac{1}{4}D_b$, and therefore, the critical length is

$$l_{cb} \cong \frac{\sigma_f D_b}{2\times 3^{1/2}\tau_i} A_{tD} \quad (48)$$

which reduces to $l_{cb}^{solid} = \sigma_f D_b/(2\times 3^{1/2}\tau_i)$ for solid fillers, and to $l_{cb}^{thin} \cong 2\sigma_f t D_b/(3^{1/2}\tau_i D)$ for thin wall tubes. Note the similarity of this equation to equation (7).

Since a compact nanotube bundle can be made very long, owing to the efficient transfer of stress between adjacent nanotubes, the maximum achievable pullout energy can be reached (assuming $l_b = l_{cb}$) for a given volume fraction V_f (equation (19))

$$G_{lcb} = \frac{V_f\sigma_f l_{cb}}{12} = \frac{V_f\sigma_f^2 D_b}{24\times 3^{1/2}\tau_i} A_{tD} \quad (49)$$

This energy is higher by a factor of $1/3^{1/2}D_b/D$ compared to the maximum pullout energy of unbundled uniformly dispersed nanotubes (equation (21)) with the same volume fraction and cross-sectional shape, each with a length $l = l_c$. This factor can be of order 10^2–10^3 for a large bundle, and is reflected in equation (44) and Fig. 17. The reason for this dramatic advantage in toughness is that the critical length of a bundle l_{cb} is much longer than that of an individual nanotube l_c, because of the high ratio $a_b/p_b \sim D_b$ in equation (47).

If the fillers composing the bundle are solid

$$G_{lcb}^{solid} = \frac{V_f\sigma_f^2 D_b}{24\times 3^{1/2}\tau_i} \quad (50)$$

similar to equation (21), and if they are thin-wall with a wall thickness t

$$G_{lcb}^{thin} \cong \frac{V_f\sigma_f^2 t}{6\times 3^{1/2}\tau_i}\frac{D_b}{D} \quad (51)$$

Under the same comparison assumptions as before ($l_b = l_{cb}$, $l = l_c$ and same V_f), the bundle's ultimate strength will be equivalent to uniformly dispersed nanotubes (equations (27) and (31)). The same is true for the stiffness, assuming the longitudinal aspect ratio is about the same for the bundle and a single nanotube ($l_b/D_b \cong l/D$) (equations (35) and (39)). Moreover, since bundles can be made very long, it is possible to reach a length l_b much higher than l_{cb}, thus approaching the maximum achievable strength and stiffness (refer to Fig. 13), a difficult goal to achieve in unbundled nanotubes.

When the nanotubes in a bundle are loosely packed (Fig. A1*a*), the matrix material partially penetrates the bundle. This phenomenon may occur in practice as a result of, for example, electrostatic charge that builds up on the nanotubes during processing or chemical treatment of the bundle. Consequently, the nanotube–matrix effective interfacial area is expanded, and the stress propagation in the bundle is modified, leading to a reduction in the effective cross-sectional area that carries the load.

Defining the effective interfacial perimeter $\langle p_b\rangle$ and the effective cross-sectional area $\langle a_b\rangle$, the effective critical length can be written as in equation (3)

$$\langle l_{cb}\rangle = \frac{2\sigma_f}{\tau_i}\frac{\langle a_b\rangle}{\langle p_b\rangle} = \frac{\sigma_f\langle D_b\rangle}{2\tau_i} \quad (52)$$

where $\langle D_b\rangle$ is the effective diameter of a bundle with a circular cross-section. Correspondingly, the effective pullout energy of the bundle, $\langle G_{lcb}\rangle = V_f\sigma_f\langle l_{cb}\rangle/12$. For a given bundle, $\langle D_b\rangle$ can be assessed by obtaining the bundle's $\langle l_{cb}^{test}\rangle$ from a fragmentation test, so that $\langle D_b\rangle \cong 2\tau_i\langle l_{cb}^{test}\rangle/\sigma_f$. The effective diameter $\langle D_b\rangle$ is evidently smaller than D_b of a tightly packed bundle (a rough estimate is $\langle D_b\rangle/D_b \sim 0.1$), and therefore the maximum achievable effective pullout energy is proportionally lower, but is still much higher than unbundled uniformly dispersed nanotubes with the same volume fraction.

While the composite strength and stiffness of tightly packed bundles were shown to be the same as for uniformly dispersed nanotubes with the same volume fraction, this is not the case for loosely packed bundles. The less efficient stress transfer between the nanotubes in a bundle means that the effective nanotube volume fraction is lower than V_f, and therefore the composite strength and stiffness will be degraded to some extent in comparison to uniformly dispersed nanotubes.

In summary, aligned tightly packed bundles have the potential of offering a significant improvement in composite toughness with respect to unbundled nanotubes, while the strength and stiffness remain unimpaired. Penetration of matrix material into the bundle may somewhat degrade the toughness, but it is still expected to remain much higher than unbundled nanotubes. Since the discussion in this appendix is generalized for any type of aligned bundle, these conclusions hold true also for small bundles, formed by agglomeration during the composite production process. This means that, from a toughness perspective, aligned agglomeration is potentially advantageous compared to uniformly dispersed nanotubes.

References

1. N. Satyanarayana, K. S. S. Rajan, S. K. Sinha and L. Shen: *Tribol. Lett.*, 2007, **27**, (2), 181–188.
2. K. L. White and H. J. Sue: *Polymer*, 2012, **53**, (1), 37–42.
3. X. M. Sui and H. D. Wagner: *Nano Lett.*, 2009, **9**, (4), 1423–1426.
4. Y. Dror, W. Salalha, R. L. Khalfin, Y. Cohen, A. L. Yarin and E. Zussman: *Langmuir*, 2003, **19**, (17), 7012–7020.
5. Y. Ji, C. Li, G. Wang, J. Koo, S. Ge, B. Li, J. Jiang, B. Herzberg, T. Klein, S. Chen, J. C. Sokolov and M. H. Rafailovich: *EPL*, 2008, **84**, (5), 56002.
6. B. G. Demczyk, Y. M. Wang, J. Cumings, M. Hetman, W. Han, A. Zettl and R. O. Ritchie: *Mater. Sci. Eng. A*, 2002, **A334**, (1–2), 173–178.
7. M. F. Yu, O. Lourie, M. J. Dyer, K. Moloni, T. F. Kelly and R. S. Ruoff: *Science*, 2000, **287**, (5453), 637–640.
8. I. Levchenko, Z.-J. Han, S. Kumar, S. Yick, J. Fang and K. Ostrikov: 'Large arrays and networks of carbon nanotubes: morphology control by process parameters', in 'Syntheses and applications of carbon nanotubes and their composites', (ed. S. Suzuki), 2013, Philadelphia, PA, InTech.
9. H. D. Wagner: *Nat. Nanotechnol.*, 2007, **2**, (12), 742–744.
10. M. H. G. Wichmann, K. Schulte and H. D. Wagner: *Compos. Sci. Technol.*, 2008, **68**, (1), 329–331.
11. N. Lachman and H. D. Wagner: *Composites Part A*, 2010, **41A**, (9), 1093–1098.
12. A. G. Evans: *J. Am. Ceram. Soc.*, 1990, **73**, (2), 187–206.
13. H. D. Wagner, P. M. Ajayan and K. Schulte: *Compos. Sci. Technol.*, 2013, **83**, 27–31.
14. H. D. Wagner: *Chem. Phys. Lett.*, 2002, **361**, (1–2), 57–61.
15. A. H. Cottrell: 'Strong solids', *Proc. R. Soc. Lond. A*, 1964, **282A**, 2–9.

Maney Publishing

16. A. Kelly and W. R. Tyson: *J. Mech. Phys. Solids*, 1965, **13**, (6), 329.
17. M. Piggott: 'Load bearing fibre composites', 475; 2002, New York, Kluwer Academic Publishers.
18. E. W. Weisstein: 'Generalized Cylinder', From MathWorld – A Wolfram Web Resource [viewed Nov 2014]; Available from: http://mathworld.wolfram.com/GeneralizedCylinder.html.
19. P. K. Mallick: 'Fiber-reinforced composites: materials, manufacturing, and design', xvii; 2008, Boca Raton, FL, CRC Press.
20. H. L. Cox: *Br. J. Appl. Phys*., 1952, **3**, 72.
21. H. D. Wagner and A. Lustiger: *Compos. Sci. Technol.*, 2009, **69**, (7–8), 1323–1325.
22. E. J. Garcia, B. L. Wardle and A. J. Hart: *Composites Part A*, 2008, **39A**, (6), 1065-1070.
23. G. Lalwani, A. M. Henslee, B. Farshid, P. Parmar, L. J. Lin, Y. X. Qin, F. K. Kasper, A. G. Mikos and B. Sitharaman: *Acta Biomater*., 2013, **9**, (9), 8365–8373.
24. M. Shtein, R. Nadiv, N. Lachman, H. D. Wagner and O. Regev: *Compos. Sci. Technol.*, 2013, **87**, 157–163.
25. Z. Yang, X. Chen, H. Nie, K. Zhang, W. Li, B. Yi and L. Xu: *Nanotechnology*, 2008, **19**, 085606.
26. C. Li, G. J. Fang, L. Y. Yuan, N. S. Liu, L. Ai, Q. Xiang, D. S. Zhao, C. X. Pan and X. Z. Zhao: *Nanotechnology*, 2007, **18**, (15), 155702.